Two classes of active transcription sites and their roles in developmental regulation

Sarah Robinson-Thiewes[a], John McCloskey[b], and Judith Kimble[b,1]

[a]Department of Genetics, University of Wisconsin–Madison, Madison, WI 53706; and [b]Department of Biochemistry, University of Wisconsin–Madison, Madison, WI 53706

Contributed by Judith Kimble, August 29, 2020 (sent for review June 25, 2020; reviewed by Aseem Ansari and Swathi Arur)

The expression of genes encoding powerful developmental regulators is exquisitely controlled, often at multiple levels. Here, we investigate developmental expression of three conserved genes, *Caenorhabditis elegans mpk-1*, *lag-1*, and *lag-3/sel-8*, which encode homologs of ERK/MAPK and core components of the Notch-dependent transcription complex, respectively. We use single-molecule FISH (smFISH) and MATLAB to visualize and quantify nuclear nascent transcripts and cytoplasmic mRNAs as a function of position along the germline developmental axis. Using differentially labeled probes, one spanning an exceptionally long first intron and the other spanning exons, we identify two classes of active transcription sites (ATS). The iATS class, for "incomplete" ATS, harbors only partial nascent transcripts; the cATS class, for "complete" ATS, harbors full-length nascent transcripts. Remarkably, the frequencies of iATS and cATS are patterned along the germline axis. For example, most *mpk-1* ATS are iATS in hermaphrodite germline stem cells, but most are cATS in differentiating stem cell daughters. Thus, *mpk-1* ATS class frequencies switch in a graded manner as stem cell daughters begin differentiation. Importantly, the patterns of ATS class frequency are gene-, stage-, and sex-specific, and cATS frequency strongly correlates with transcriptional output. Although the molecular mechanism underlying ATS classes is not understood, their primary difference is the extent of transcriptional progression. To generate only partial nascent transcripts in iATS, progression must be slowed, paused, or aborted midway through the gene. We propose that regulation of ATS class can be a critical mode of developmental gene regulation.

active transcription site | germ cell development | ERK/MAPK

The control of gene expression is central to animal development and homeostasis. To achieve that control, an increasingly complex choreography of regulatory steps dictates when, where, and how much mRNA is produced. Transcriptional initiation has taken center stage as the key step in regulating gene expression for years (1), but other downstream mechanisms have now joined initiation on that stage. Most relevant to this work is transcriptional progression through the gene, which affects generation of a complete nascent transcript. A classic example of regulation at this step of transcriptional progression occurs in *Drosophila* embryos, where the cell cycle is too short to complete transcription through unusually long Hox genes before the cell divides (2, 3). A more broadly used case is the regulated release from transcriptional pauses that occur ∼20 to 60 bp after initiation, the promoter-proximal pause (4). Transcriptional progression can be deduced with "-omic" methods, such as PRO-seq or NET-seq (5, 6), or with imaging methods, such as single-molecule fluorescence in situ hybridization (smFISH) or live imaging (7). One advantage of smFISH is that transcription of endogenous genes can be assessed in their native context with single-cell and single-molecule resolution. This work began with an smFISH investigation of active transcription site or sites (ATS) and transcriptional yields at key regulatory genes during development. Our analyses led to discovery of two distinct ATS classes and what we propose is a case of regulated transcriptional progression.

Our studies have been conducted in the adult *Caenorhabditis elegans* gonad, which is well suited to smFISH (8) and where germ cell development occurs linearly along the distal–proximal axis. Germline stem cells (GSCs) reside within their niche at the distal end, and GSC daughters mature progressively toward gametogenesis as they move from the niche and ultimately reach the other end (Fig. 1*A*). Previous studies in this tissue revealed a gradient of Notch-dependent transcriptional bursts at the Notch target gene, *sygl-1* (8–10). Here, we focus on transcription of three other genes that regulate GSC self-renewal or differentiation (Fig. 1*B*). The *lag-1* and *lag-3/sel-8* (henceforth *lag-3*) genes encode core components of the Notch transcriptional activation complex, which promotes GSC self-renewal in response to signaling from the niche (11–13). The *mpk-1* gene encodes ERK/MAP kinase (14, 15), which promotes several aspects of germline differentiation: sperm/oocyte fate specification (16, 17), progression through meiotic prophase, and oogenesis (18–20). We emphasize that our approach queries transcription at endogenous genes in wildtype animals; our results therefore avoid potentially confounding effects of transgenes, inserted tags, and reporter constructs.

To obtain a high-resolution and quantitative view of transcription during development, we coupled smFISH with a MATLAB image analysis code to score RNAs with 3D resolution in the germline tissue, as done previously for *sygl-1* (8, 10). Using differentially labeled probe sets to either the 5′ half to two

Significance

Transcription occurs at chromosomal sites known as active transcription sites (ATS). We report that ATS can exist in two classes when assessed at key regulatory genes in their natural context: these "iATS" and "cATS" possess incomplete and complete nascent transcripts, respectively. Frequencies of the two classes are patterned within the developing tissue in a gene-, developmental stage-, and sex-specific manner, revealing ATS class regulation. Moreover, cATS frequency, not iATS frequency, corresponds to mRNA abundance, indicating that regulation of ATS class impacts gene expression. The iATS signature—presence of a long first intron but lacking exons—suggests slowing or pausing of transcriptional progression midway through the gene. We suggest that ATS class regulation can pattern gene expression during development.

Author contributions: S.R.-T. and J.K. designed research; S.R.-T. performed research; S.R.-T. and J.M. contributed new reagents/analytic tools; S.R.-T. analyzed data; and S.R.-T. and J.K. wrote the paper.

Reviewers: A.A., St. Jude Children's Research Hospital; and S.A., University of Texas MD Anderson Cancer Center.

The authors declare no competing interest.

[1]To whom correspondence may be addressed. Email: jekimble@wisc.edu.

This article contains supporting information online at https://www.pnas.org/lookup/suppl/doi:10.1073/pnas.2013163117/-/DCSupplemental.

First published October 8, 2020.

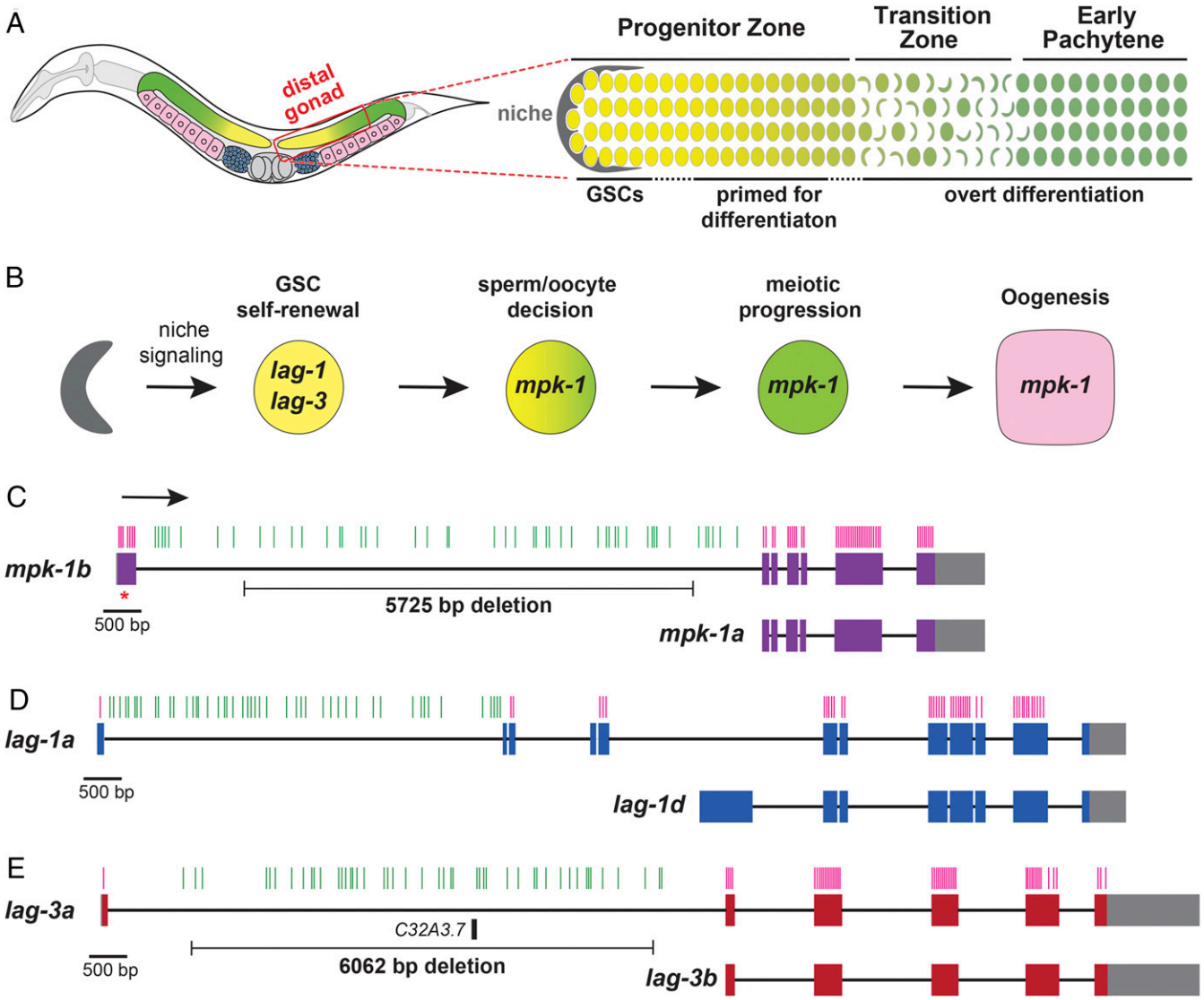

Fig. 1. *C. elegans* germline anatomy and key regulatory genes. (*A, Left*) Adult hermaphrodite has two U-shaped gonadal arms (in colors). The distal gonad (red square) houses germ cells that are either dividing (yellow) or in early meiotic prophase (green); proximal germ cells make oocytes (pink). Sperm (blue) were made as larvae. (*A, Right*) Development in distal gonad. The progenitor zone (PZ) includes germline stem cells (GSCs) within their niche (gray) and stem cell daughters primed to differentiate; upon leaving the PZ, germ cells enter meiotic prophase (green crescents). (*B*) Key regulators relevant to this work. (*C–E*) Gene architecture: boxes, exons; lines, introns. Exons include coding regions (gene-specific colors) and untranslated regions (UTRs; gray). Direction of transcription is the same for all genes (arrow in *C*). Vertical lines indicate sites of individual smFISH probes; probe sets target either the large first intron (green) or all exons (magenta). Red asterisk marks site of 1 bp frame-shifting insertion in *mpk-1b* first exon, used as control for *mpk-1* exon probe specificity. Deletions in *mpk-1* and *lag-3* long first introns were used as control for intron probe specificity. The *lag-1* gene makes four isoforms (*lag-1a-d*); for simplicity, *lag-1a* represents *lag-1a-c*, which differ in size of exons 2 and 3. The *lag-3a* first intron contains predicted ncRNA *C32A3.7*.

thirds of each gene (spanning the long first intron) or the remaining 3′ part (the exons, most of which are 3′ to the intron), we found two distinct ATS classes that differ in transcriptional progression. One class, iATS for "incomplete" ATS, harbors partial nascent transcripts; the other class, cATS for "complete" ATS, harbors full-length nascent transcripts. The iATS do not reflect a promoter-proximal pause, which generates a very short transcript that would not be seen with an intron probe (*Discussion*). Remarkably, the frequencies of these ATS classes are gene-, position-, and sex-specific, suggesting developmental regulation. Most strikingly, iATS and cATS frequencies are reciprocally graded for two genes in the stem cell region in a manner consistent with the graded expression of those genes. We propose that regulated changes in transcriptional progression, inferred from changes in the frequency of ATS class, drives the developmental expression of these genes.

Results

Experimental Design and a Modified MATLAB Code. Our experimental design took advantage of the simple architecture of the *C. elegans* adult germline (Fig. 1*A*), the ability to visualize transcription at high resolution in this tissue using smFISH (8, 10), and genes with long first introns that encode key regulators of germline development (Fig. 1*B*). The *mpk-1*, *lag-1*, and *lag-3* first introns are 8.2 kb, 6 kb, and 8.5 kb, respectively. We used Stellaris Probe Designer to create two probe sets for each gene, spanning either the long first intron and thus covering the 5′ half to two thirds of each gene or all exons and thus covering the remaining 3′ part of the gene (Fig. 1 *C–E*). Each set included 47

or 48 individual probes (detailed in Dataset S1). The intron and exon probe sets were labeled with different fluorophores to generate distinct signals (Fig. 2 *A*–*C* and *SI Appendix*, Figs. S1*A*, S2*A*, and S3*A*). Probe specificities were confirmed by inhibiting transcription with α-amanitin to ensure detection of RNA rather than DNA (*SI Appendix*, Figs. S1*B*, S2*B*, and S3*B*), intron-specific deletions to ensure specificity of the intron probe signal (*mpk-1* and *lag-3* only; an analogous *lag-1* deletion could not be isolated; *SI Appendix*, Figs. S1*C* and S3*C*), and a frame-shift mutant (*mpk-1*) or RNAi (*lag-1*, *lag-3*) to ensure specificity of the exon probe signal (*SI Appendix*, Figs. S1*D*, S2 *C* and *D*, and S3 *D* and *E*). The legends of *SI Appendix*, Fig. S1–S3, provide gene-specific details of these specificity assays.

A previously published MATLAB code (used to analyze transcription in the *C. elegans* progenitor zone) defined ATS as nuclear spots with overlapping exon and intron probe signals (8). However, a preliminary inspection by eye of the smFISH images for *mpk-1*, *lag-1*, and *lag-3* transcripts revealed two types of nuclear spots, both with morphology and size of an ATS. We categorize these two types as "cATS" and "iATS" (Fig. 2*D*). cATS are detected with overlapping signals from the exon and intron probe sets, while iATS are detected uniquely with the intron probe set. The finding of these two ATS types caused us to modify the original code. Briefly, the new code detects nuclear signals independently for the exon and intron probe sets, it determines if the two signals are overlapping to assign them as a cATS or iATS, and it identifies cytoplasmic mRNA, all within the 3D gonad (*SI Appendix*, Fig. S4, and see *SI Appendix*, *Methods*). During this code revision, we asked how many nuclear spots were seen with each probe set, without taking into consideration any overlap, and found that the intron probe detected more spots than the exon probe for all three genes (Fig. 2*E*). To test whether the abundance bias of intron spots might reflect fluorophore differences, we tested *mpk-1* probe sets with swapped fluorophores, but the intron spot abundance bias did not change (Fig. 2*E*). To validate our modified MATLAB code, we tested it by rescoring previously published images of *sygl-1* smFISH and obtained results equivalent to a previous report (*SI Appendix*, Fig. S5) (8). The new code thus scores cATS and iATS with spatial resolution.

Transcriptional Probabilities and Yields in the Progenitor Zone. We analyzed *mpk-1*, *lag-1*, and *lag-3* transcription in the adult hermaphrodite Progenitor Zone (PZ), where GSCs reside distally and more proximal GSC daughters become primed for differentiation (21–23). Position within the PZ was scored as the number of germ cell diameters (gcds) or "rows" along the distal–proximal axis from the distal end, by convention. For this study, we focused on the distal-most 12 rows of the PZ, a region with roughly 150 germ cells that divide asynchronously every ~6 h on average (24) and move proximally at a rate of ~0.4 to 1 row per hour (22). Importantly, a germ cell's state—naïve and stem cell-like or triggered to differentiate—corresponds to its position along the axis (Fig. 3*A*).

We first determined the percentage of germ cells harboring any ATS, cell row by cell row, along the PZ developmental axis. The ATS scored in this initial analysis include both cATS and iATS, and thus reveal genes that have not only initiated transcription but also elongated far enough for detection with smFISH probes. The percentage of cells with any ATS therefore provides a measure of transcriptional probability, as established previously (8, 9, 25). The *mpk-1*, *lag-1*, and *lag-3* genes were all transcribed actively across the distal PZ, with 60 to 70% of cells possessing either a cATS or iATS (Fig. 3*B* and *SI Appendix*, Fig. S6 *A*–*C*). For comparison, the Notch-activated *sygl-1* gene produces ATS in ~65% of the distal germ cells within the niche

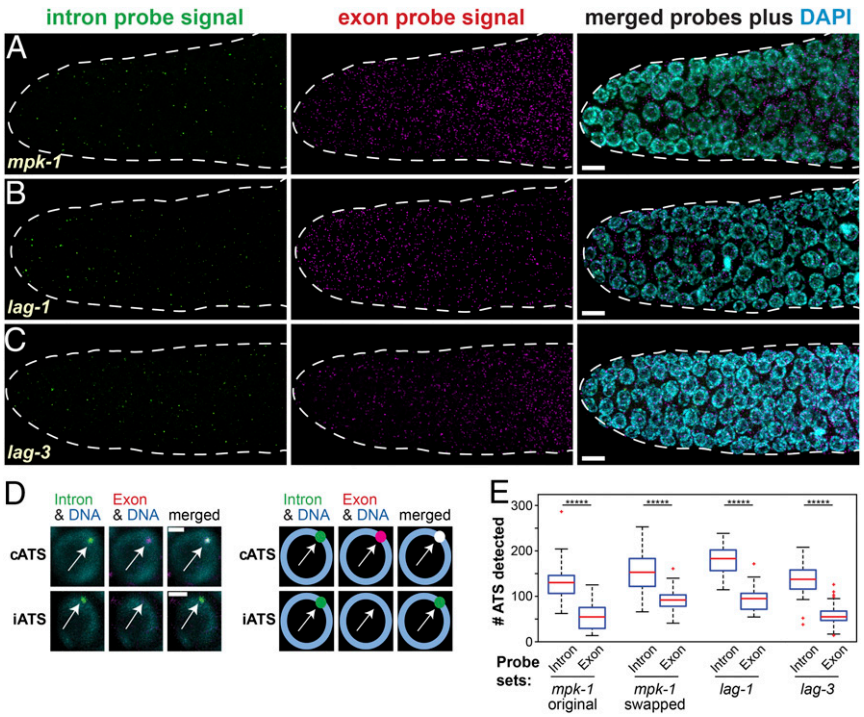

Fig. 2. Identification of two classes of active transcription sites (ATS). (*A*–*C*) Maximum projections of smFISH images. (*Left*) Intron probe set signals (green), (*Middle*) exon probe set signals (magenta), and merge of both signals with DAPI (cyan). (Scale bar, 5 μm.) (*D*) Two ATS classes: (*Left*) images and (*Right*) cartoons. A cATS (complete ATS) is visualized by overlapping intron and exon probe signals; an iATS (incomplete ATS) is visualized by the intron probe signal alone. (*E*) ATS numbers, regardless of class, detected with either the intron probe set (intron) or exon probe set (exon) for each gene. Overlaps of intron-detected and exon-detected spots were not determined in this analysis. To test if the high number of intron-detected spots reflected fluorophore bias, the fluorophores conjugated to the original *mpk-1* intron and exon probes were swapped (*****$P < 0.0000001$, Student's *t* test).

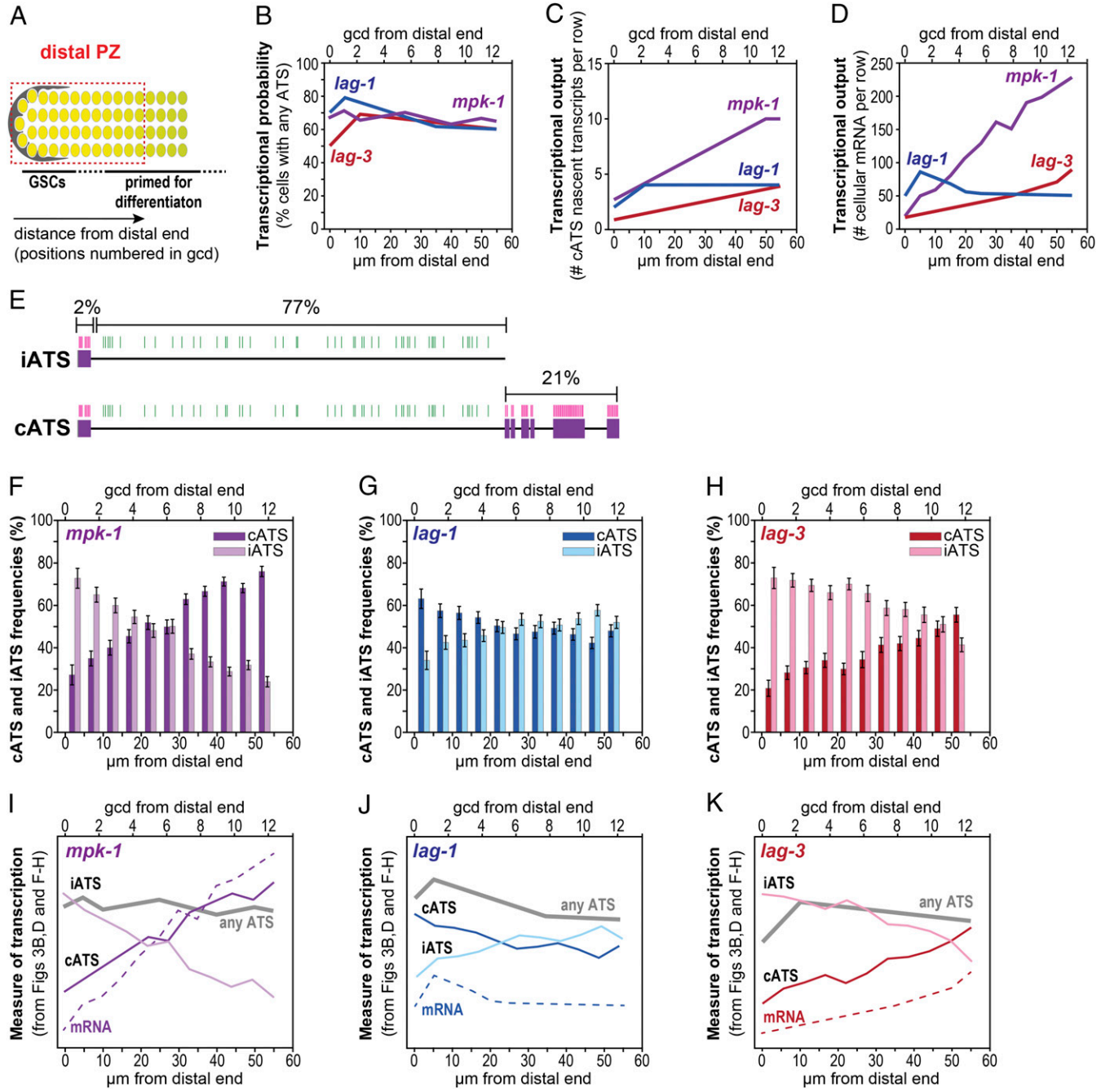

Fig. 3. Expression of *mpk-1*, *lag-1*, and *lag-3* in the distal Progenitor Zone (PZ). (*A*) Region scored (dashed red box) extends 12 germ cell diameters (gcds) into the PZ from the niche (gray). Numbers indicate positions as gcds along the distal–proximal axis, starting from the distal end according to convention; MATLAB score position in micrometers from the distal end, with each gcd averaging ∼4.4 μm in this region (8). (*B–D* and *F–K*) The *x*-axis shows position in both gcds (*Top*) and micrometers (*Bottom*). Numbers of gonads scored: *mpk-1*, $n = 37$; *lag-1*, $n = 36$; and *lag-3*, $n = 32$. (*B*) Transcriptional probability measured as percentage of cells with at least one ATS, including both iATS and cATS. Line plots are derived from data in *SI Appendix*, Fig. S6 *A–C*. Total numbers of cells scored: *mpk-1*, $n = 6{,}065$; *lag-1*, $n = 5{,}981$; and *lag-3*, $n = 4{,}472$. (*C*) Transcriptional output measured as total number of nascent transcripts at cATS per cell row. Analysis was limited to cATS as explained in the text and detailed in *SI Appendix*, *Methods*. Line plots are derived from data in *SI Appendix*, Fig. S6 *G–I*. (*D*) Transcriptional output measured as total number of cellular mRNAs per cell row; mRNAs in rachis were excluded. Germ cell boundaries were determined from MATLAB-generated Voronoi cells as described in *SI Appendix*, *Methods*. Line plots are derived from data in *SI Appendix*, Fig. S6 *J–L*. Data for number of mRNAs per cell are in *SI Appendix*, Fig. S6 *M–O*. (*E*) Detection of nascent transcripts at iATS (*Top*) and cATS (*Bottom*). iATS are seen uniquely with the intron probe set, whereas cATS are seen with overlapping exon and intron probe sets. The *mpk-1* intron probe set spans 77% of the full-length transcript (excluding 3′UTR); by contrast, the exon probe set spans only 23%. (*F–H*) iATS and cATS frequencies as a function of position. Each bar shows percentage of total ATS that are cATS (darker bars) or iATS (lighter bars). Numbers of total ATS (cATS plus iATS) scored: *mpk-1*, $n = 5{,}699$; *lag-1*, $n = 6{,}610$; and *lag-3*, $n = 4{,}200$. SEs are shown. (*I–K*) Measures of transcription taken from panels above and combined to highlight patterns of graded increase, decrease, or relative uniformity; individual lines represent quite different measures, and specific values are therefore not comparable. Transcriptional probability (gray line) is from *B*, cellular mRNA abundance per row (dashed line) is from *D*, and cATS frequency (dark colored line) and iATS frequency (lighter colored line) are from *G–I*. The original panels show *y*-axis value ranges.

but <5% outside the niche, as previously reported (8). We also scored how many individual ATS were seen in each nucleus as a function of position along the axis. As expected for genes that transcribe in bursts within an actively dividing cell population, the numbers of individual ATS per cell varied between zero and four (*SI Appendix*, Fig. S6 *D–F*). The higher percentage in the most distal germ cells for *lag-1* ATS and lower percentage in the same region for *lag-3* ATS are reproducible but not understood. Most importantly, all three genes are actively engaged in transcription across the distal PZ.

We next scored two measures of transcriptional productivity as a function of position in the PZ: the number of nascent transcripts at cATS (Fig. 3*C* and *SI Appendix*, Fig. S6 *G–I*) and number of mRNAs in the cytoplasm (Fig. 3*D* and *SI Appendix*, Fig. S6 *J–O*). Measurement of nascent transcript abundance was limited to cATS because it could be estimated by comparing intensity values of exon probe spots at cATS in the nucleus and exon probe dots at single mRNAs in the cytoplasm. While this strategy misses nascent transcripts at iATS, the compared values rely on the same probe, same fluorophore, and same image. Both the number of *mpk-1* and *lag-3* nascent transcripts increased steadily as germ cells moved along the PZ axis, while the number of *lag-1* nascent transcripts increased initially and then leveled off (Fig. 3*C*). Following those trends, *mpk-1* and *lag*-3 mRNA numbers also increased along the axis, while numbers of *lag-1* mRNAs were more level (Fig. 3*D*). The pattern of *lag-1* mRNA abundance conforms for the most part with an independent report published recently (26). Most strikingly, the nearly uniform transcriptional probabilities for *mpk-1* and *lag-3* (Fig. 3*B*) did not match their gradually increasing transcriptional outputs across the PZ axis (Fig. 3 *C* and *D*).

Frequency of One ATS Class, the cATS, Corresponds to mRNA Yield. Why might transcriptional probability and output have distinct patterns for a given gene? We considered the possibility that the frequency of the two ATS classes, iATS and cATS (Fig. 2), underlie the explanation. iATS are uniquely detected with the first intron probe, so nascent transcripts at iATS have elongated through much of the long intron, but not the downstream exons (Fig. 3 *E*, *Top*). By contrast, cATS are detected with both exon and intron probes, so nascent transcripts at cATS must have elongated through both the long intron and the downstream exons (Fig. 3 *E*, *Bottom*). Because iATS and cATS reveal transcription sites dominated by different extents of transcriptional progression, cATS would be expected to yield a more robust transcriptional output than iATS. Based on that idea, we determined the frequencies of each ATS class, measured as a percentage of all ATS, and asked if their frequencies change along the PZ developmental axis. One might have thought that iATS and cATS frequencies would simply reflect the extent of sequence covered by each probe set. If that were the case, they would be the same regardless of position. However, iATS and cATS frequencies had gene-specific patterns along the PZ axis (Fig. 3 *F–H*). For example, *mpk-1* cATS frequency increased steadily from ~30% distally to ~75% at row 12, and iATS frequency decreased correspondingly (Fig. 3*F*). A similar trend was found for *lag-3* (Fig. 3*H*), but the *lag-1* cATS frequency initially decreased and then leveled off across the PZ (Fig. 3*G*). These patterns suggest that transcriptional progression is gene-specific and changes as germ cells move through the PZ. A logical extension of that idea is that the pattern of only one class, the cATS with their full- or nearly full-length transcripts, is responsible for the pattern of mRNA production. That prediction was borne out by comparing patterns of ATS, cATS, iATS, and mRNAs in gene-specific graphs (Fig. 3 *I* and *J*) and finding positive correlations between cATS frequency and mRNA number and negative correlations between iATS frequency and mRNA number (Table 1). We conclude that cATS frequency, not iATS frequency, drives mRNA output as germ cells mature through the PZ (*Discussion*).

***mpk-1*, *lag-1*, and *lag-3* Transcription in the Early Pachytene Region.** We next investigated transcription of the same three genes in a different region of the gonad, where germ cells have begun to differentiate. Specifically, we focused on 12 rows of germ cells that begin at the proximal boundary of the Transition Zone (TZ) and extend into the pachytene region (Fig. 4*A*). Germ cells here have entered the pachytene stage of meiotic prophase and begun oogenesis. For simplicity, we refer to the region as EP for Early Pachytene. Though germ cells are not dividing mitotically, they move proximally through the EP at a rate of ~1 row per hour (21, 24) and progressively mature as they move along the distal–proximal axis.

Analyses in the EP paralleled those in the distal PZ (*SI Appendix*, Fig. S7, shows representative smFISH images). The *mpk-1*, *lag-1*, and *lag-3* genes were actively transcribed across the region: the percentages of cells with any ATS ranged from ~50% to 80% (Fig. 4*B* and *SI Appendix*, Fig. S8 *A–C*), and ATS numbered zero to four per nucleus as expected (*SI Appendix*, Fig. S8 *D–F*). The number of nascent transcripts at cATS was steady across the region for each gene (Fig. 4*C* and *SI Appendix*, Fig. S8 *G–I*), while mRNA numbers were essentially uniform or increased slightly (Fig. 4*D* and *SI Appendix*, Fig. S8 *J–O*). Strikingly and in contrast to the PZ, most ATS were cATS throughout the EP region (Fig. 4 *E–G*). Display of the various measures of transcription in a single graph highlights their similarity (Fig. 4 *H–J*). Again, high cATS frequencies match abundance of cytoplasmic mRNAs. Thus, the ATS class frequencies and hence transcriptional progression appear relatively uniform for these genes as they move through early pachytene.

Deletions in the *mpk-1* Long First Intron Have Either Minor or No Detectable Germline Defects. We considered the idea that the size or content of the long first intron of each gene might influence the pattern of cATS frequency in the PZ. Introns can contain regulatory elements that affect numerous aspects of the transcription process, including elongation and splicing (2, 27–32). To address this issue, we focused on *mpk-1* for two reasons. First, the *mpk-1b* isoform is the principal and likely only *mpk-1* transcript in the germline (Fig. 1*C*) (33, 34). As a result, *mpk-1* smFISH in the germline scores this isoform specifically. By contrast, tissue specificity is unknown for the isoforms of the other genes (Fig. 1 *D* and *E*). Second, a 5.7 kb deletion in the *mpk-1* intron (Fig. 1*C*) is homozygous viable. Therefore, the regulatory effects of potential elements within the *mpk-1* long first intron can be investigated with mutants. By contrast, an analogous deletion in *lag-3* (Fig. 1*D*) is embryonic lethal and the analogous *lag-1* intron deletion could not be recovered. Briefly, we generated three 1 kb deletions in different areas of the long first intron, but these deletions did not affect the ATS class pattern, frequency, or *mpk-1* gene expression (*SI Appendix*, Figs. S9 andS10). "Analyses of *mpk-1* intron deletion mutants" in the *SI Appendix* provides details of these experiments.

***mpk-1* Developmental Pattern of cATS Frequency Is Sex-Specific.** Finally, we asked if the low *mpk-1* cATS frequency found in hermaphrodite GSCs reflects a GSC-related developmental control and the high cATS frequency in hermaphrodite EPs reflects a differentiation developmental control. If this were the case, similar frequencies would be expected in male GSCs, which also reside in the distal PZ, and in the male EP (Fig. 5*A*, red boxes) (10). However, the male pattern of cATS frequency differed dramatically from that in hermaphrodites. The cATS frequency was ~50% in male GSCs and dropped from ~80% at the TZ/EP boundary to ~40% by row 12 in the EP (Fig. 5*C*). The *mpk-1* cATS frequency pattern is therefore sexually dimorphic (Fig. 5 *D*

Table 1. Pearson's correlation tests between distinct measures of transcription

Comparison	Gene	Correlation coefficient (*r*)	*P* value
% cells with any ATS vs	*mpk-1*	0.0157	0.7456
# mRNA in cells	*lag-1*	0.0725	0.1362
	lag-3	−0.0594	0.0594
% ATS that are cATS vs	*mpk-1*	0.4872	7.5725×10^{-28}
# mRNA in cells	*lag-1*	0.1272	0.0081
	lag-3	0.4448	4.6640×10^{-20}
% ATS that are iATS vs	*mpk-1*	−0.4520	9.6179×10^{-24}
# mRNA in cells	*lag-1*	−0.1149	0.0169
	lag-3	−0.3836	6.5252×10^{-15}
# cATS nascent transcripts vs	*mpk-1*	0.8214	1.9340×10^{-106}
# mRNA in cells	*lag-1*	0.3807	2.3929×10^{-16}
	lag-3	0.8074	3.9855×10^{-86}

and *E*). The male EP decrease in cATS frequency matches well with the previously reported decrease in MPK-1 protein abundance in the same region (16). We suggest that the sexually dimorphic patterns in cATS frequency reflect sex-specific changes in transcriptional progression related to specification of the sperm fate in the male PZ and production of maternal RNAs in the hermaphrodite EP (*Discussion*).

Discussion

This study analyzes expression of three key regulatory genes during *C. elegans* germline development, using smFISH to visualize nascent transcripts at active transcription sites (ATS) and mRNAs, both with single-cell resolution. Our results lead to three conclusions. First, we identify distinct ATS classes: iATS with partial nascent transcripts and cATS with full-length nascent transcripts. Second, we find that the frequencies of these ATS classes change in gene- and sex-specific fashion along the germline developmental axis, suggesting developmental regulation. Finally, we show that only one ATS class, the cATS, correlates with transcriptional productivity, suggesting an impact of ATS class on gene expression.

Two ATS Classes with Distinct Extents of Transcriptional Progression and Transcriptional Output. Classically, ATS are thought to harbor multiple transcripts that vary in degree of completeness (35–37). The discovery of iATS and cATS demonstrates that ATS can exist in different states with distinct extents of transcriptional progression through a gene. The iATS are detected with the intron probe set spanning the 5′ half to two thirds of each gene, but they are not detected with the exon probe spanning the 3′ third to half of each gene; therefore, the iATS class makes only partial transcripts. The cATS, by contrast, are detected with both intron and exon probe sets and must make complete or nearly complete transcripts, likely in addition to partial transcripts (Fig. 6*A*). This interpretation is consistent with previous studies that used smFISH to investigate transcriptional progression (7, 37–39). Moreover, alternative explanations seem unlikely. The lack of an overlapping exon signal at iATS might be explained if the spliced long intron were tethered to the site while full-length transcripts were released rapidly. However, introns are typically degraded quickly (40) or moved to nuclear speckles for degradation (41–43), and a rapid release of full-length transcripts is inconsistent with the negative correlation between iATS frequency and transcriptional output (Table 1). We therefore favor the idea that iATS and cATS differ in their extents of transcriptional progression (Fig. 6*A*).

We do not understand the mechanism responsible for formation of these two ATS classes. The simplest explanation is that transcriptional elongation is slowed or paused at iATS, perhaps in the long first intron. That slowing or pausing cannot be the same as promoter-proximal pausing, which occurs ∼20 to 60 bp downstream of transcriptional initiation and would not generate a transcript detectable with the first intron probe (4, 5, 44). If pausing does occur at iATS, it could be coupled to splicing (45–48). However, splicing pauses detected to date in other systems are short, on the order of seconds to minutes (49–51), but could be longer if regulated. Another plausible explanation is that transcription is aborted at iATS. Abortive transcription occurs in *Drosophila* embryos, where mitosis truncates transcription of very long genes in cells with very short cell cycles (2, 3, 28, 52, 53). However, in the iATS reported in our work, elongation through each gene is predicted to take <15 min, based on rates of 1 to 4 kb/s (37, 49, 50), far less than the ∼6-h cell cycle in the progenitor zone (24); thus, iATS are unlikely to be the result of aborted transcription at mitosis. Differentiating among these various mechanisms is challenging in the *C. elegans* germline, and iATS per se have not yet been reported in cultured cells. Nonetheless, although speculative, we suggest that iATS result from transcriptional pausing, perhaps during RNAP II elongation or splicing of the long first intron.

Graded cATS Frequency Is Coupled to a Graded Transcriptional Output. One of our most striking findings is that frequencies of the two ATS classes, iATS and cATS, are patterned in development. Whereas the probability of a nucleus harboring any ATS was essentially the same for all germ cells in the two regions investigated, the frequencies of the two ATS classes changed dramatically and reciprocally as germ cells mature. Indeed, the *mpk-1* and *lag-3* frequencies were clearly graded in the hermaphrodite progenitor zone. For both genes, iATS frequency started high in GSCs within the niche and dropped as their daughters left the niche and moved through the progenitor zone; conversely, cATS frequency started low and increased across the same region. These reciprocally graded iATS and cATS frequencies likely reflect graded and regulated changes in the ability of an ATS to complete transcription through the gene.

An important corollary of the iATS class, with its partial transcripts, is that the existence of an active transcription site per se does not ensure production of mRNAs. The iATS frequency had a pattern opposite to that of transcriptional yield, measured both as production of full-length nascent transcripts and mature mRNAs, whereas the cATS frequency pattern aligned well with these two measures of transcriptional output. Future smFISH studies must therefore take into account not only the presence of an ATS, but the ATS class and its productivity. This caution may be most important for genes with long introns or perhaps simply long genes. We suspected that some aspect of the long first intron might be critical for producing the two ATS classes but were not able to identify it with designer deletions. Regardless, for the key genes investigated in this work, we suggest that the regulated

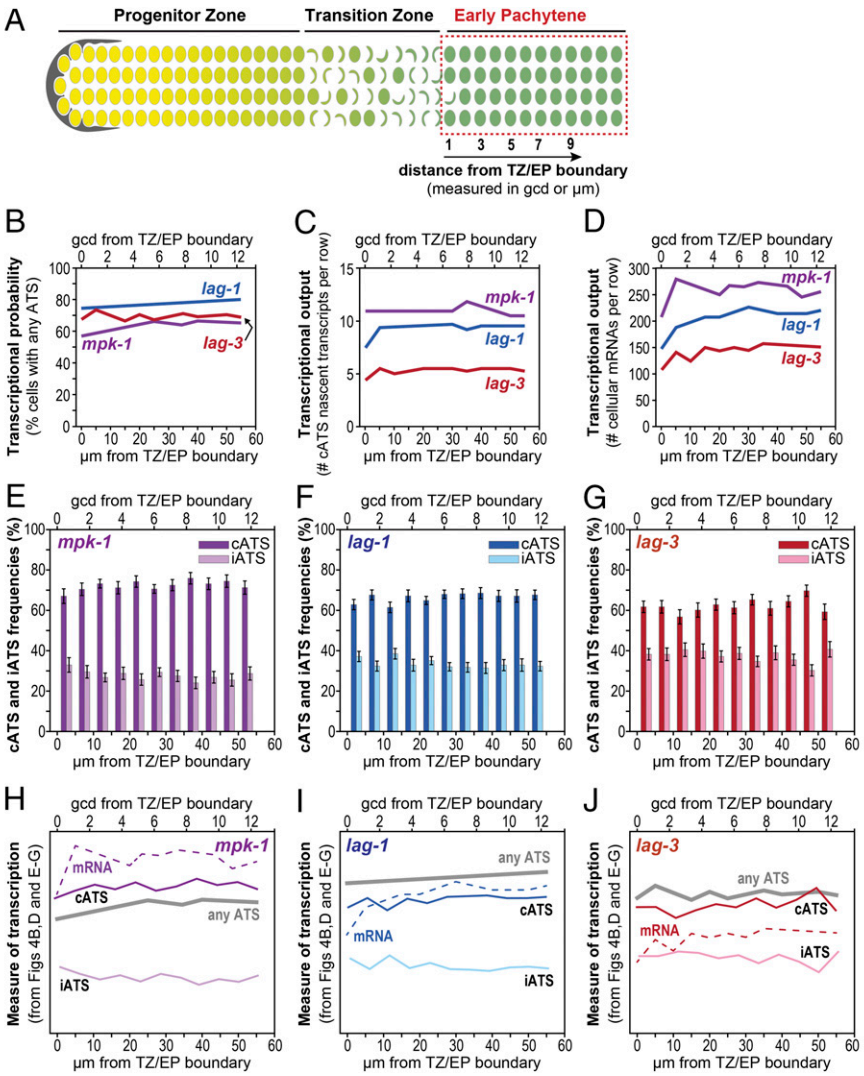

Fig. 4. Transcription of *mpk-1*, *lag-1*, and *lag-3* in Early Pachytene (EP) region. (*A*) Region scored (dashed red box) extends 12 gcds from the TZ/EP boundary. Numbers mark gcd positions, starting at TZ/EP boundary; each gcd averages ~4.4 µm in this region. *SI Appendix*, Fig. S7, provides smFISH images. (*B–J*) Quantification of transcripts. Numbers of gonads scored: *mpk*-1, $n = 36$; *lag-1*, $n = 36$; and *lag-3*, $n = 37$. The *x*-axis shows position as both gcds (*Top*) and micrometers (*Bottom*) from TZ/EP boundary. (*B*) Transcriptional probability measured as percent cells with one or more ATS of either class. Total cell numbers scored: *mpk-1*, $n = 6{,}249$; *lag-1*, $n = 6{,}064$; and *lag-3*, $n = 4{,}625$. Line plots are from data in *SI Appendix*, Fig. S8 *A–C*. (*C*) Transcriptional output measured as total nascent transcripts at cATS per cell row (see text and *SI Appendix, Methods*). Line plots are from data in *SI Appendix*, Fig. S8 *G–I*. (*D*) Transcriptional output measured as total number of mRNAs in cells per row (cells defined as in Fig. 2*D*); mRNAs in rachis were excluded. Line plots are from data in *SI Appendix*, Fig. S8 *J–L*. Data for mRNA number per cell are shown in *SI Appendix*, Fig. S8 *M–O*. (*E–G*) ATS class frequencies as a function of position. Total number of ATS (either class) scored: *mpk-1*, $n = 5{,}749$; *lag-1*, $n = 10{,}118$; and *lag-3*, $n = 4{,}730$. (*H–J*) Measures of transcription taken from panels above and combined to highlight patterns; individual lines represent different measures, and specific values are therefore not comparable. Transcriptional probability (gray line) is from *B*, number of mRNAs in cells (dashed colored line) are from *D*, and cATS frequency (dark colored line) and iATS frequency (light colored line) are from *E–G*. The original panels show *y*-axis value ranges.

balance between cATS and iATS classes is an important factor in driving gene expression.

ATS Classes Are Gene-, Stage-, and Sex-Specific during Germline Development. The three genes investigated in this work—*mpk-1*, *lag-1*, and *lag-3*—encode key regulators of development (*Introduction*). In the germline tissue, they regulate stem cell maintenance, sex determination, and several steps of differentiation (Fig. 1*B*); elsewhere, they regulate embryogenesis and postembryonic somatic development (54, 55). Here we consider how the patterns of ATS class frequency relate to germline function. This is most straightforward in the hermaphrodite Early Pachytene region where germ cells act as nurse cells for oocytes (56). All three genes produce maternal mRNAs (57), consistent with their high cATS frequency and abundant transcriptional yield to load maternal mRNAs into the oocyte.

The patterns of cATS frequency are more nuanced in the Progenitor Zone. We first consider *lag-1* and *lag-3*, which encode essential components of the Notch-dependent transcription factor complex and are required for GSC maintenance (8, 11, 13, 58). Consistent with that role, the *lag-1* cATS frequency and transcriptional output are higher in GSCs than in the more proximal PZ (this work), and LAG-1 protein is expressed similarly (26). More puzzling is the *lag-3* cATS pattern, which is low in GSCs even though LAG-3 protein must function there to maintain GSCs. The explanation may rely on LAG-3 functioning in a nuclear complex with the Notch intracellular domain (NICD) (13), with abundance of nuclear NICD vanishingly low

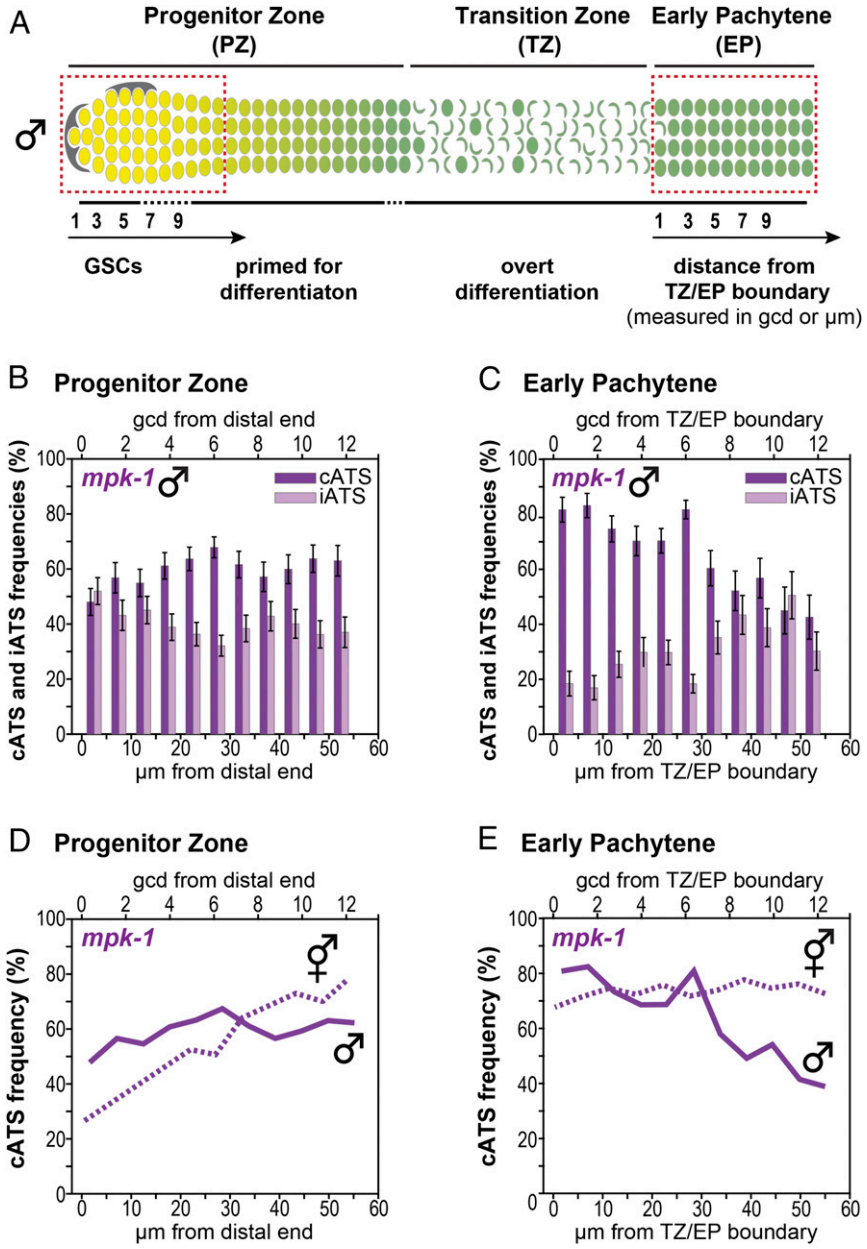

Fig. 5. Male *mpk-1* ATS pattern. (*A*) Male gonad architecture with two somatic niche cells (gray), longer Progenitor and Transition Zones than hermaphrodites (66), but similar GSC pool size in the two sexes (10). Red boxes mark regions analyzed: the first 12 cell rows of PZ and first 12 cell rows of Early Pachytene (EP) region. (*B* and *D*) PZ data; conventions as in Fig. 3. Number of gonads scored, $n = 24$. (*C* and *E*) EP data; conventions as in Fig. 4. Number of gonads, $n = 22$. (*B* and *C*) iATS and cATS frequencies in the PZ (*B*) and EP (*C*). Total number of ATS scored in PZ, $n = 2{,}195$; in EP, $n = 1{,}350$. (*D* and *E*) Male *mpk-1* cATS frequency (solid purple) compared to hermaphrodite cATS frequency (dashed purple) in the PZ (*D*) and EP (*E*). Hermaphrodite data are taken from Fig. 3*J* for PZ and Fig. 4*H* for the EP.

(59, 60). We suspect that LAG-3 abundance must be kept low to work with its low-abundance NICD companion for Notch-dependent transcriptional activation. Indeed, mammalian Mastermind-like (MAML), a LAG-3 ortholog (61–64), is often overexpressed in cancers (62, 65). Perhaps the *lag-3* cATS frequency must be kept low to prevent overexpression and tumorigenesis.

The *C. elegans* ERK/MAPK ortholog, *mpk-1*, functions at several steps of germline differentiation: sperm fate specification, meiotic progression, and oocyte maturation (16–20). These functions all rely on a single germline-specific isoform, *mpk-1b* mRNA, which, in hermaphrodites, generates low MPK-1B protein in the PZ and increasing MPK-1B as germ cells progress through differentiation (16, 33). As shown in Fig. 6*B*, the pattern of *mpk-1* cATS frequency and transcriptional output in hermaphrodites conforms to the pattern of MPK-1B protein expression and its established functions in meiotic progression and oocyte maturation. Given its prominent role in germline differentiation, *mpk-1* expression might have been kept low in GSCs to maintain stem cells. However, germline sexual identity is established within the PZ (17, 66), and *mpk-1* promotes sperm fate (16). Indeed, *mpk-1* cATS frequency was sexually dimorphic: 25% in GSCs of oogenic but ~50% in GSCs of spermatogenic germlines (Fig. 6*B*). The low cATS frequency seen in

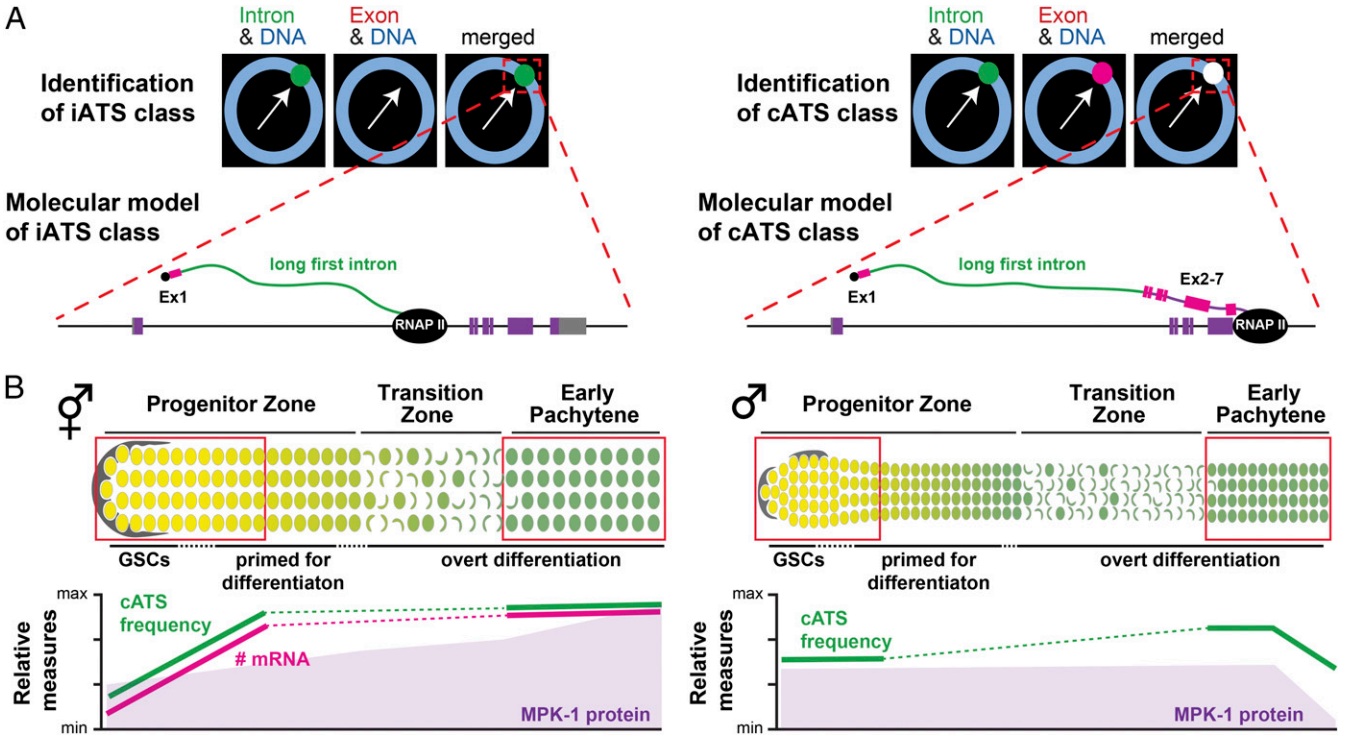

Fig. 6. Models for ATS classes and their regulation in development. (*A*) Simple molecular models of iATS and cATS. (*Left*) iATS nascent transcripts are detected with the long first intron probe set and therefore likely consist of the first exon (Ex1) and much of the long first intron, but not more downstream exons (Ex2-7). We show one incomplete nascent transcript during transcriptional elongation by RNA polymerase II (RNAP II) for simplicity, but iATS could result from slowed or paused transcriptional elongation, slowed or paused splicing, or aborted transcription, with each mechanism leading to different partial nascent transcripts (*Discussion*). (*Right*) cATS nascent transcripts are detected with both intron and exon probe sets. We show one complete nascent transcript with the first exon, long first intron, and all downstream exons for simplicity, but cATS likely include a spectrum of partial and complete transcripts. (*B*) Biological models for *mpk-1* ATS class frequency having a critical role in developmental gene expression. Developmental stages shown above correspond to patterns of ATS class frequency, transcriptional output, and protein expression shown below (*Discussion*).

hermaphrodite GSCs is therefore not required for stem cell maintenance but instead is consistent with preventing sperm fate specification in oogenic adult hermaphrodites. Although the abundance and activity of MPK-1/ERK are also regulated posttranscriptionally and posttranslationally (33, 67), regulation of ATS class, and hence regulation of transcriptional progression, emerges as its earliest point of developmental control.

Future Directions. A deeper understanding of ATS classes and their regulation is a challenge for future studies. One key question is whether iATS form at other genes, in other tissues, and in other species. The literature reveals plausible iATS candidates in *Drosophila* and mouse (3, 27), but those studies used different methods and their iATS equivalence is uncertain. A second key question is the mechanism regulating ATS class. If found in cultured cells, this question can be addressed with powerful biochemical and genomic methods. The *C. elegans* iATS reported here occur in a minority of cells within the germline tissue, a substantial barrier for -omics methods. However, mechanism can be approached in *C. elegans* with more refined smFISH analyses to probe the possibility of a transcriptional pause in iATS and live imaging to ask about transcriptional or pause dynamics. Regardless, identification of a graded developmental transition from iATS to cATS opens the possibility of a previously unrecognized mode of transcriptional regulation.

Materials and Methods

Detailed materials and methods are provided in *SI Appendix, Methods*. Briefly, all strains were maintained at 20 °C (68) unless otherwise indicated. Most experiments were done using wildtype N2 animals, but *SI Appendix*, Table S1 provides strain names and genotypes. All mutations were made in otherwise wildtype animals using CRISPR (69, 70), with guides listed in *SI Appendix*, Table S2. Statistical tests were performed in MATLAB: Student's *t* test (ttest2 function) and Pearson's correlation tests (corr function). Significance cutoff of $P \leq 0.01$ was used.

Data Availability. MATLAB codes are deposited and publicly avaliable at https://github.com/robinson-thiewes/Robinson-thiewes-PNAS-codes- (DOI: 10.5281/zenodo.4007918). All study data are included in the article and supporting information. Raw Matlab workspaces are available upon request.

ACKNOWLEDGMENTS. We thank members of the Kimble laboratory, Wickens laboratory, David Brow, Bob Landick, Daniel Panaccione, and Aaron Hoskins for thoughtful discussions. We thank Brian Carrick, Sarah Crittenden, and Tina Lynch for critical manuscript reading; Laura Vanderploeg for help with figures; and ChangHwan Lee for sharing expertise about smFISH, MATLAB, and *lag-3* RNAi. S.R.-T. was supported by the NSF Graduate Research Fellowship under Grant DGE-1256259 and NIH Predoctoral Training Grant in Genetics 5T32GM007133. J.K. was an HHMI Investigator and is now supported by NIH Grant R01 GM134119. Any opinion, findings, and conclusions or recommendations expressed in this material are those of the authors(s) and do not necessarily reflect the views of the National Science Foundation.

1. M. Mannervik, Y. Nibu, H. Zhang, M. Levine, Transcriptional coregulators in development. *Science* **284**, 606–609 (1999).
2. D. Gubb, Intron-delay and the precision of expression of homoeotic gene products in Drosophila. *Dev. Genet.* **7**, 119–131 (1986).
3. A. W. Shermoen, P. H. O'Farrell, Progression of the cell cycle through mitosis leads to abortion of nascent transcripts. *Cell* **67**, 303–310 (1991).
4. K. Adelman, J. T. Lis, Promoter-proximal pausing of RNA polymerase II: Emerging roles in metazoans. *Nat. Rev. Genet.* **13**, 720–731 (2012).

5. I. Jonkers, J. T. Lis, Getting up to speed with transcription elongation by RNA polymerase II. *Nat. Rev. Mol. Cell Biol.* **16**, 167–177 (2015).
6. L. S. Churchman, J. S. Weissman, Nascent transcript sequencing visualizes transcription at nucleotide resolution. *Nature* **469**, 368–373 (2011).
7. X. Pichon, M. Lagha, F. Mueller, E. Bertrand, A growing toolbox to image gene expression in single cells: Sensitive approaches for demanding challenges. *Mol. Cell* **71**, 468–480 (2018).
8. C. Lee, E. B. Sorensen, T. R. Lynch, J. Kimble, *C. elegans* GLP-1/Notch activates transcription in a probability gradient across the germline stem cell pool. *eLife* **5**, e18370 (2016).
9. C. Lee, H. Shin, J. Kimble, Dynamics of Notch-dependent transcriptional bursting in its native context. *Dev. Cell* **50**, 426–435.e4 (2019).
10. S. L. Crittenden *et al*., Sexual dimorphism of niche architecture and regulation of the *Caenorhabditis elegans* germline stem cell pool. *Mol. Biol. Cell* **30**, 1757–1769 (2019).
11. E. J. Lambie, J. Kimble, Two homologous regulatory genes, lin-12 and glp-1, have overlapping functions. *Development* **112**, 231–240 (1991).
12. S. Christensen, V. Kodoyianni, M. Bosenberg, L. Friedman, J. Kimble, lag-1, a gene required for lin-12 and glp-1 signaling in Caenorhabditis elegans, is homologous to human CBF1 and Drosophila Su(H). *Development* **122**, 1373–1383 (1996).
13. A. G. Petcherski, J. Kimble, LAG-3 is a putative transcriptional activator in the C. elegans Notch pathway. *Nature* **405**, 364–368 (2000).
14. M. R. Lackner, K. Kornfeld, L. M. Miller, H. R. Horvitz, S. K. Kim, A MAP kinase homolog, mpk-1, is involved in ras-mediated induction of vulval cell fates in Caenorhabditis elegans. *Genes Dev.* **8**, 160–173 (1994).
15. Y. Wu, M. Han, Suppression of activated Let-60 ras protein defines a role of Caenorhabditis elegans Sur-1 MAP kinase in vulval differentiation. *Genes Dev.* **8**, 147–159 (1994).
16. M. H. Lee *et al*., Multiple functions and dynamic activation of MPK-1 extracellular signal-regulated kinase signaling in Caenorhabditis elegans germline development. *Genetics* **177**, 2039–2062 (2007).
17. C. T. Morgan, D. Noble, J. Kimble, Mitosis-meiosis and sperm-oocyte fate decisions are separable regulatory events. *Proc. Natl. Acad. Sci. U.S.A.* **110**, 3411–3416 (2013).
18. D. L. Church, K. L. Guan, E. J. Lambie, Three genes of the MAP kinase cascade, mek-2, mpk-1/sur-1 and let-60 ras, are required for meiotic cell cycle progression in Caenorhabditis elegans. *Development* **121**, 2525–2535 (1995).
19. A. L. Lopez 3rd *et al*., DAF-2 and ERK couple nutrient availability to meiotic progression during Caenorhabditis elegans oogenesis. *Dev. Cell* **27**, 227–240 (2013).
20. S. Arur *et al*., MPK-1 ERK controls membrane organization in C. elegans oogenesis via a sex-determination module. *Dev. Cell* **20**, 677–688 (2011).
21. S. L. Crittenden, K. A. Leonhard, D. T. Byrd, J. Kimble, Cellular analyses of the mitotic region in the Caenorhabditis elegans adult germ line. *Mol. Biol. Cell* **17**, 3051–3061 (2006).
22. S. Rosu, O. Cohen-Fix, Live-imaging analysis of germ cell proliferation in the C. elegans adult supports a stochastic model for stem cell proliferation. *Dev. Biol.* **423**, 93–100 (2017).
23. O. Cinquin, S. L. Crittenden, D. E. Morgan, J. Kimble, Progression from a stem cell-like state to early differentiation in the C. elegans germ line. *Proc. Natl. Acad. Sci. U.S.A.* **107**, 2048–2053 (2010).
24. E. J. A. Hubbard, T. Schedl, Biology of the caenorhabditis elegans germline stem cell system. *Genetics* **213**, 1145–1188 (2019).
25. J. R. Chubb, T. Trcek, S. M. Shenoy, R. H. Singer, Transcriptional pulsing of a developmental gene. *Curr. Biol.* **16**, 1018–1025 (2006).
26. J. Chen *et al*., GLP-1 Notch-LAG-1 CSL control of the germline stem cell fate is mediated by transcriptional targets lst-1 and sygl-1. *PLoS Genet.* **16**, e1008650 (2020).
27. Y. Takashima, T. Ohtsuka, A. González, H. Miyachi, R. Kageyama, Intronic delay is essential for oscillatory expression in the segmentation clock. *Proc. Natl. Acad. Sci. U.S.A.* **108**, 3300–3305 (2011).
28. I. A. Swinburne, P. A. Silver, Intron delays and transcriptional timing during development. *Dev. Cell* **14**, 324–330 (2008).
29. I. A. Swinburne, D. G. Miguez, D. Landgraf, P. A. Silver, Intron length increases oscillatory periods of gene expression in animal cells. *Genes Dev.* **22**, 2342–2346 (2008).
30. M. Chorev, L. Carmel, The function of introns. *Front. Genet.* **3**, 55 (2012).
31. A. B. Rose, Introns as gene regulators: A brick on the accelerator. *Front. Genet.* **9**, 672 (2019).
32. J. Parenteau *et al*., Introns are mediators of cell response to starvation. *Nature* **565**, 612–617 (2019).
33. M. H. Lee *et al*., Conserved regulation of MAP kinase expression by PUF RNA-binding proteins. *PLoS Genet.* **3**, e233 (2007).
34. S. Robinson-Thiewes, B. Dufour, P.-O. Martel *et al*, Non-autonomous regulation of germline stem cell proliferation by somatic MPK-1/MAPK activity in C. elegans. bioRxiv:2020.08.24.265249 (August 24, 2020)
35. S. L. Mcknight, O. L. Miller, Ultrastructural patterns of RNA synthesis during early embryogenesis of Drosophila melanogaster. *Cell Mass Inst. Technol.* **8**, 309–315 (1976).
36. A. M. Femino, F. S. Fay, K. Fogarty, R. H. Singer, Visualization of single RNA transcripts in situ. *Science* **280**, 585–590 (1998).
37. X. Darzacq *et al*., In vivo dynamics of RNA polymerase II transcription. *Nat. Struct. Mol. Biol.* **14**, 796–806 (2007).
38. A. Coté, C. Coté, S. Bayatpour *et al*, The spatial distributions of pre-mRNAs suggest post-transcriptional splicing of specific introns within endogenous genes. bioRxiv: 2020.04.06.028092 (April 7, 2020).
39. C. R. Bartman *et al*., Transcriptional burst initiation and polymerase pause release are key control points of transcriptional regulation. *Mol. Cell* **73**, 519–532.e4 (2019).
40. J. Q. Clement, L. Qian, N. Kaplinsky, M. F. Wilkinson, The stability and fate of a spliced intron from vertebrate cells. *RNA* **5**, 206–220 (1999).
41. E. Daguenet *et al*., Perispeckles are major assembly sites for the exon junction core complex. *Mol. Biol. Cell* **23**, 1765–1782 (2012).
42. A. P. Dias, K. Dufu, H. Lei, R. Reed, A role for TREX components in the release of spliced mRNA from nuclear speckle domains. *Nat. Commun.* **1**, 97 (2010).
43. L. Galganski, M. O. Urbanek, W. J. Krzyzosiak, Nuclear speckles: Molecular organization, biological function and role in disease. *Nucleic Acids Res.* **45**, 10350–10368 (2017).
44. R. M. Sheridan, N. Fong, A. D'Alessandro, D. L. Bentley, Widespread backtracking by RNA Pol II is a major effector of gene activation, 5′ pause release, termination, and transcription elongation rate. *Mol. Cell* **73**, 107–118.e4 (2018).
45. R. D. Alexander, S. A. Innocente, J. D. Barrass, J. D. Beggs, Splicing-dependent RNA polymerase pausing in yeast. *Mol. Cell* **40**, 582–593 (2010).
46. A. Mayer *et al*., Native elongating transcript sequencing reveals human transcriptional activity at nucleotide resolution. *Cell* **161**, 541–554 (2015).
47. T. Nojima *et al*., Mammalian NET-seq reveals genome-wide nascent transcription coupled to RNA processing. *Cell* **161**, 526–540 (2015).
48. T. Saldi, M. A. Cortazar, R. M. Sheridan, D. L. Bentley, Coupling of RNA polymerase II transcription elongation with pre-mRNA splicing. *J. Mol. Biol.* **428**, 2623–2635 (2016).
49. R. M. Martin, J. Rino, C. Carvalho, T. Kirchhausen, M. Carmo-Fonseca, Live-cell visualization of pre-mRNA splicing with single-molecule sensitivity. *Cell Rep.* **4**, 1144–1155 (2013).
50. J. Singh, R. A. Padgett, Rates of in situ transcription and splicing in large human genes. *Nat. Struct. Mol. Biol.* **16**, 1128–1133 (2009).
51. T. Alpert, L. Herzel, K. M. Neugebauer, Perfect timing: Splicing and transcription rates in living cells. *Wiley Interdiscip. Rev. RNA* **8**, 10.1002/wrna.1401 (2017).
52. W. Tadros, H. D. Lipshitz, The maternal-to-zygotic transition: A play in two acts. *Development* **136**, 3033–3042 (2009).
53. J. C. Kwasnieski, T. L. Orr-Weaver, D. P. Bartel, Early genome activation in *Drosophila* is extensive with an initial tendency for aborted transcripts and retained introns. *Genome Res.* **29**, 1188–1197 (2019).
54. J. R. Priess, "Notch signaling in the C. elegans embryo" in *WormBook*, ed. The C. elegans Research Community, www.wormbook.org (June 25, 2005), 10.1895/wormbook.1.4.1.
55. P. W. Sternberg, "Vulval development" in *WormBook*, ed. The C. elegans Research Community, www.wormbook.org (June 25, 2005), doi/10.1895/wormbook.1.6.1.
56. U. Wolke, E. A. Jezuit, J. R. Priess, Actin-dependent cytoplasmic streaming in C. elegans oogenesis. *Development* **134**, 2227–2236 (2007).
57. M. Stoeckius *et al*., Global characterization of the oocyte-to-embryo transition in Caenorhabditis elegans uncovers a novel mRNA clearance mechanism. *EMBO J.* **33**, 1751–1766 (2014).
58. A. M. Kershner, H. Shin, T. J. Hansen, J. Kimble, Discovery of two GLP-1/Notch target genes that account for the role of GLP-1/Notch signaling in stem cell maintenance. *Proc. Natl. Acad. Sci. U.S.A.* **111**, 3739–3744 (2014).
59. S. L. Crittenden, E. R. Troemel, T. C. Evans, J. Kimble, GLP-1 is localized to the mitotic region of the C. elegans germ line. *Development* **120**, 2901–2911 (1994).
60. E. B. Sorensen, H. S. Seidel, S. L. Crittenden *et al*., A toolkit of tagged glp-1 alleles reveals strong glp-1 expression in the germline, embryo, and spermatheca. *MicroPubl Biol.*, 10.17912/micropub.biology.000271 (2020).
61. Y. Zhao *et al*., The notch regulator MAML1 interacts with p53 and functions as a coactivator. *J. Biol. Chem.* **282**, 11969–11981 (2007).
62. L. Wu, J. D. Griffin, Modulation of Notch signaling by mastermind-like (MAML) transcriptional co-activators and their involvement in tumorigenesis. *Semin. Cancer Biol.* **14**, 348–356 (2004).
63. A. S. McElhinny, J. L. Li, L. Wu, Mastermind-like transcriptional co-activators: Emerging roles in regulating cross talk among multiple signaling pathways. *Oncogene* **27**, 5138–5147 (2008).
64. M. Kitagawa, Notch signalling in the nucleus: Roles of Mastermind-like (MAML) transcriptional coactivators. *J. Biochem.* **159**, 287–294 (2015).
65. M. M. Forghanifard *et al*., Expression analysis elucidates the roles of MAML1 and Twist1 in esophageal squamous cell carcinoma aggressiveness and metastasis. *Ann. Surg. Oncol.* **19**, 743–749 (2012).
66. D. E. Morgan, S. L. Crittenden, J. Kimble, The C. elegans adult male germline: Stem cells and sexual dimorphism. *Dev. Biol.* **346**, 204–214 (2010).
67. D. S. Yoon, M. A. Alfhili, K. Friend, M.-H. Lee, MPK-1/ERK regulatory network controls the number of sperm by regulating timing of sperm-oocyte switch in C. elegans germline. *Biochem. Biophys. Res. Commun.* **491**, 1077–1082 (2017).
68. S. Brenner, The genetics of Caenorhabditis elegans. *Genetics* **77**, 71–94 (1974).
69. A. Paix *et al*., Scalable and versatile genome editing using linear DNAs with microhomology to Cas9 Sites in Caenorhabditis elegans. *Genetics* **198**, 1347–1356 (2014).
70. G. A. Dokshin, K. S. Ghanta, K. M. Piscopo, C. C. Mello, Robust genome editing with short single-stranded and long, partially single-stranded DNA donors in *Caenorhabditis elegans*. *Genetics* **210**, 781–787 (2018).